Generation and control of helium-filled soap bubbles for large-scale PIV

Engler Faleiros, David; Tuinstra, Marthijn; Sciacchitano, Andrea; Scarano, Fulvio

Publication date
2018

Document Version
Final published version

Published in
Proceedings of the 19th international symposium on application of laser and imaging techniques to fluid mechanics

Generation and control of helium-filled soap bubbles for large-scale PIV

David E. Faleiros[1,2,*], Marthijn Tuinstra[1], Andrea Sciacchitano[2], Fulvio Scarano[2]
1: Helicopters and Aeroacoustics Department, Netherlands Aerospace Centre (NLR), the Netherlands
2: Faculty of Aerospace Engineering, Delft University of Technology, the Netherlands
* Correspondent author: david.engler.faleiros@nlr.nl

Keywords: HFSB, neutrally buoyant particles, large-scale PIV

ABSTRACT

The operating regimes of an orifice-type helium-filled soap bubbles (HFSB) generator are investigated to characterize the properties of the resulting tracers. The geometrical properties of the bubbles as well as the production rate are studied with high-speed shadowgraphy. The weight of the tracers relative to the mass of displaced air is determined by Particle Image Velocimetry (PIV) measurements along the stagnation streamline ahead of a cylinder. The latter data yield the particle time response for several combinations of air, helium and soap flow rates. The bubble production rate appears to increase linearly with the air flow rate, whereas the bubble volume is found to be directly proportional to the ratio of helium and air volume flow rates. The HFSB tracing capability approaches that of an ideal tracer (i.e. shortest response time), when the volume flow rate of helium is approximately one thousandfold the soap flow rate. This study provides guidelines for operating HFSB generation systems within large-scale PIV experiments.

1. Introduction

The use of helium-filled soap bubbles (HFSB) as flow tracers for flow visualization dates back to the early work of Pounder et al. (1956). In comparison to other tracers used in air flows, HFSB are large particles (~ 0.5 to 5 mm) that can be illuminated with conventional light sources and observed from a distance of several meters. Compared to micrometric droplets used for PIV, soap bubbles reflect 10^4 times more light (Caridi, 2018). This enables large-scale Particle Image Velocimetry (PIV) measurements, where the finite scattering efficiency of tracer particles usually limits the measured domain (Raffel, 2007). The initial efforts to use HFSB for quantitative velocity measurements were discouraged due to difficulties of generating bubbles that could accurately follow the flow (Kerho & Bragg, 1994). The tracing fidelity of HFSB was later demonstrated for sub-millimeter bubbles in the steady flow upstream of a cylinder (Scarano et al. 2015), where the bubbles followed closely the streamlines obtained with fog droplets. A time response of 10 μs was inferred from the measured slip velocity within the known acceleration.

More recently the tracing fidelity of HFSB has been inquired within turbulent boundary layers (Faleiros et al. 2018). The good accuracy in the measurements of mean velocity and its fluctuations is paving the way to the application of HFSB in a wide range of flow regimes and especially for the study of large-scale aerodynamic problems (automotive, aerospace, wind energy and sports, among others).

The aerodynamic behavior of HFSB is closest to ideal when the tracer density equals that of the air flow (neutrally-buoyant particle). Moreover, the bubble needs to be sufficiently smaller than the relevant flow structure. To achieve neutral buoyancy the mass flows of helium and soap are carefully controlled to match the density of air.

HFSB are generated with an orifice-type bubble generator (Okuno et al. 1993, Bosbach et al. 2009, see Fig. 1) that coaxially supplies air, helium and bubble fluid solution (BFS). The film of BFS is extruded from the edge of the coaxial duct by the surrounding air flow. During this process the film accelerates and reduces its thickness towards the region of maximum speed across the orifice. Depending on the production regime, the instability of the liquid film leads to a regular formation of soap bubbles enclosing helium. The orifice-type bubble generator achieves production rates in the order of 10^4 bubbles/second (10^2 higher than previous designs, Okuno et al. 1993). The latter, however, remains relatively low to seed wind tunnel flows for most PIV experiments. Following the study of Caridi et al. (2016) a wind tunnel stream can be seeded using a single generator by accumulating the bubbles in a reservoir and then rapidly releasing them. The system was demonstrated for large-scale PIV measurements over a wind turbine. However, the efficiency of tracers transport and distribution in the stream was shown to be very low. Consequently, the attention has moved towards the realization of devices operating simultaneously tens or hundreds of generators. In this case, the assumption that all generators operate exactly under the same regime is often violated. As a result, the tracer distribution exhibits a wide dispersion, resulting in large uncertainties of their aerodynamic behavior and of the associated measurement.

Even for a single generator, flow visualizations have shown that the generation of bubbles might occur in two regimes: bubbling and jetting (Morias et al. 2016). During bubbling, a bubble emerges regularly from the orifice exit. In the jetting regime, the cylindrical soap film extends beyond the nozzle exit and eventually breaks up into bubbles in a less regular process. A monodisperse distribution is beneficial to the accuracy of PIV measurements as particle size and weight determine their time response. This is best achieved in the bubbling production regime. Morias et al. (2016) and Faleiros et al. (2018) have observed that in the bubbling regime HFSB exhibit a relatively small dispersion in terms of diameter standard deviation (approx. 10% of the

bubble diameter). In contrast time-response can vary in the range from 10 to 40 μs. In the jetting regime, the HFSB size and time response are expected to have greater variations. Morias et al. (2016) found that increasing the air flow rate, the dispersion of bubble size approximately doubled, which was ascribed to the transition to the jetting regime. A detailed characterization of the latter transition is not present in the literature. The characterization of the HFSB production and their properties is the objective of the present study.

Some important guidelines for the production of neutrally-buoyant HFSB have already been discussed in the literature. Bosbach et al. (2009), Scarano et al. (2015) and Morias et al. (2016) used a similar device and reported similar flow rates of BFS and helium (5 ml/h and 5 l/h, respectively) resulting in the production of neutrally buoyant HFSB. The flow rate of air, however, was varied more broadly from 60 l/h (Bosbach at al. 2009) up to 160 l/h (Morias et al. 2016). There is also some discrepancy in the reported bubble diameters and production rate. The bubble diameter varied from 0.23 mm (Bosbach et al. 2009) up to 0.55 mm (Morias et al. 2016 and Faleiros et al. 2018). The bubble production rate varied from 50,000 bubbles per second (Morias et al. 2016 and Caridi et al. 2016) up to 200,000 bubbles per second (Bosbach et al. 2009). Also in this respect, the literature lacks a systematic study that characterizes the relation between the fluid supply rates, the resulting production regime and the rate at which bubbles are released.

A thorough description of the HFSB generator is herewith intended to permit the diffusion and standardization of these tracers for PIV users that aim at performing large-scale experiments in the low-speed aerodynamic regimes. Proper control of the generation of conventional micrometer oil particles is nowadays guaranteed for measurements obtained at smaller scales, where a detailed study of atomizer nozzles (Kähler et al. 2002) delivers the relevant parameters affecting the particle size distribution.

For a given geometry of the generator, the input parameters affecting the HFSB production are the fluid properties and volume flow rates of air, helium and BFS. The system output is monitored in terms of working regime (bubbling or jetting), average production rate, particle size, inferred weight and time response. The knowledge of such parameters allows for a well-designed PIV experiment and a good estimation of the experimental uncertainty.

2. Instrumentation

The main bubble generator employed in the experiments is an NLR design (Fig. 1, left) of 1 mm orifice diameter based on the HFSB-GEN-V11 developed at TU Delft. Another bubble generator geometry (Fig. 1, right) based on a DLR design (Bosbach et al. 2009) has also been tested. For

the latter generator, since geometry modifications were more easily performed, three different orifice diameters d_o have been tested (0.75 mm, 1 mm and 1.5 mm). The flow in the NLR generator approaches the orifice at an angle of 35° with the flow direction and turns around a sharp edge at the orifice. In comparison to a nozzle shape in which the flow approaches the orifice at 90°, the latter has the advantage of avoiding soap accumulation in the separated regions at the straight angles.

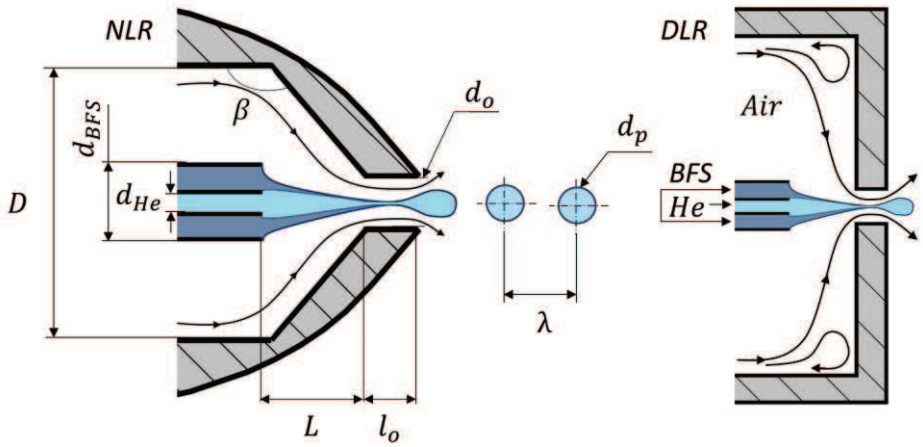

Nozzle	NLR	DLR
β	125°	90°
D	4	10
d_{BFS}	2	2
d_{he}	0.5	0.5
d_o	1	{0.75, 1, 1.5}
L	2	2
l_o	1	1

Fig. 1 Schematic sectional view of the bubble generators used in the experiments (not to scale). Dimensions in mm.

The gases and soap mass flows are tuned, respectively, using El-Flow Select and Mini Cori Flow mass flow controllers from Bronkhorst. The bubble fluid solution used is the SAI 1035 from Sage Action, Inc. The properties of the fluids are given in Table 1. The images were recorded with a LaVision HighSpeedStar 5 CMOS camera (1024×1024 pixels, 12 bits, 20 µm pixel pitch). The laser used during PIV measurements is a diode pumped Litron Nd:YLF LDY304 (2 × 30 mJ/pulse at 1 kHz).

Fluid	Density ρ (kg/m³)	Dynamic viscosity µ (Pa.s)	Surface tension γ (mN/m)
Air	1.20	1.8×10-5	-
Helium	0.17	2.0×10-5	-
BFS	1,124	8.0×10-3	27.5

Table 1 Fluid properties at 20° C and 1 atm.

3. Neutral buoyancy

The mass conservation for the production of HFSB of volume V_p and density ρ_p is

$$f V_p \rho_p = Q_{He}\rho_{He} + Q_{BFS}\rho_{BFS} \qquad (1)$$

in which f is the HFSB production rate and Q the fluid volume flow rates. Assuming $fV_p = Q_{He}$ (negligible soap film thickness), the density of the bubble is given as

$$\rho_p = \rho_{He} + \rho_{BFS}\frac{Q_{BFS}}{Q_{He}} \qquad (2)$$

Thus, the neutral buoyancy condition ($\rho_p = \rho_{air}$) at T = 20°C is in theory satisfied when $Q_{He}/Q_{BFS} \cong 1{,}080$. The production of neutrally buoyant bubbles is a requirement for an accurate PIV measurement, because the particle time response to fluid acceleration is linearly related to the weight of the bubble, or more specifically with the difference in density between particle and fluid. In the Stokes regime, the time response of a particle of diameter d_p in a fluid of density ρ and dynamic viscosity μ is (Adrian and Westerweel, 2011):

$$\tau_p = \frac{(\rho_p - \rho)d_p^2}{18\mu} \qquad (3)$$

The time response of the tracers can also be inferred as the ratio between slip velocity and fluid acceleration. The technique used to measure the latter properties is based on the dynamics forces that a spherical particle (Mei, 1996) undergoes during deceleration in the steady laminar flow ahead of a circular cylinder (Scarano et al. 2015). The approach has been adopted in several studies (Morias et al. 2016, Faleiros et al. 2018) producing estimations of the particles response time consistent with the bubbles characteristics. The slip velocity is obtained from the difference between the bubbles velocity obtained from particle tracking velocimetry (PTV) and the velocity field from PIV (DEHS particles are used as tracers).

Measurements of HFSB time response were performed in the small anechoic wind tunnel KAT of the Netherlands Aerospace Centre (NLR) using a cylinder of 50 mm diameter, spanning the 38×51 cm² test-section. The wind tunnel speed was set at 30 m/s. The resulting deceleration ahead of the cylinder is in the order of 600g (~ 5,000 m/s²). A total of 35 combinations of volume flow rates of air (65 - 160 l/h), helium (4 – 21 l/h) and soap (3.5 - 11 ml/h) were tested. For details of the experimental set-up and processing of the data the reader is referred to Faleiros et al. (2018).

The effect of particle time response can be observed qualitatively through the streamlines in front of the cylinder (Fig. 2). The black streamlines show the reference measurements obtained using DEHS (τ_p = 2 μs). Nearly neutrally buoyant HFSB ($\tau_p = 23\ \mu s$) follow closely the reference streamlines. Heavier-than-air bubbles ($\tau_p = 144\ \mu s$) take longer to respond to the acceleration due to their inertia and, therefore, the particles approach closer to the cylinder before turning sideways. Lighter-than-air bubbles ($\tau_p = -92\ \mu s$, negative sign indicating lighter than air), respond faster to flow acceleration than air itself, as a result of the lower inertia force compared to the pressure gradient generated by the presence of the object.

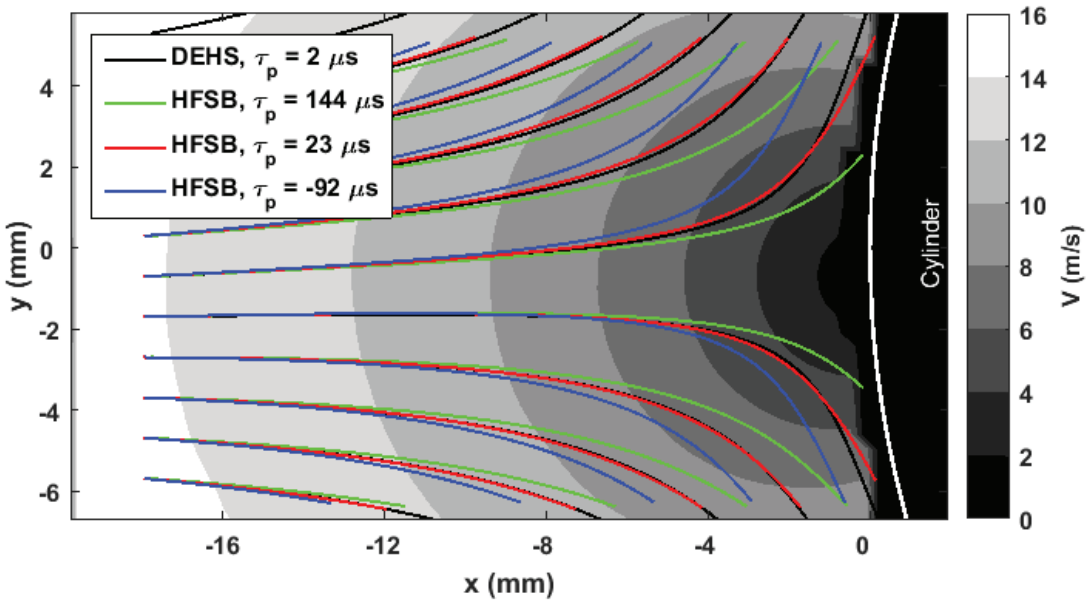

Fig. 2 Flow field ahead of the circular cylinder obtained from PIV measurements (velocity contours and solid black lines as streamlines). Trajectories of neutrally buoyant HFSB tracers (solid red lines).

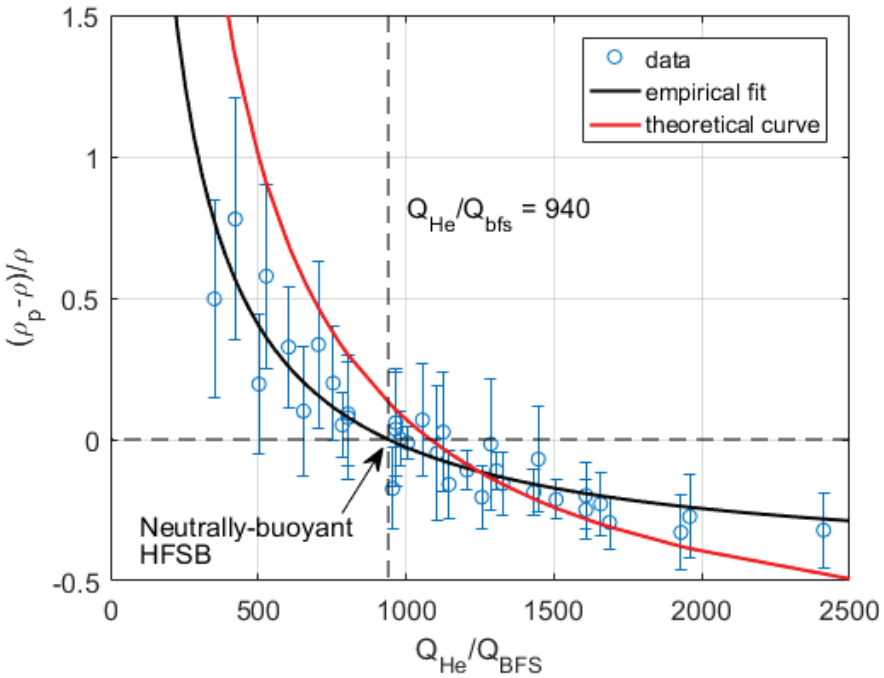

Fig. 3 Normalized HFSB density difference

The bubble diameter (Fig. 11) can be measured through the distance between two glare points formed by each bubble (Dehaeck et al. 2005). The bubble density is then estimated from eq. (2). The dependency of the normalized density difference $\bar{\rho} = (\rho_p - \rho)/\rho$ on Q_{He}/Q_{BFS} is shown in Fig. 3. The empirical fitted curve ($\bar{\rho}$ = -0.46 + 433Q_{He}/Q_{BFS}) has a similar shape as the theoretical curve . The point where the fitted curve crosses the neutrally-buoyant line ($\bar{\rho} = 0$), gives the

empirical ratio of helium and soap volume flow rates that results in neutrally-buoyant HFSB: $Q_{He}/Q_{BFS} = 940$. The difference between empirical and theoretical curves could be due to non-negligible effect of added-mass force (Faleiros et al. 2018) causing the theoretical value to be slightly overestimated, i.e. particles follow the flow better than predicted by Stokes flow theory. Nevertheless, this would not change the neutral buoyancy condition ($\bar{\rho} = 0$, $\tau_p = 0$). The latter might be due to spillage of soap, which would thus cause the neutral buoyancy condition to be achieved with less amount of helium than expected.

4. Visualization Technique

The measurements were performed via shadow visualization of the bubbles at the exit of the generator. The high speed camera was placed perpendicular to the bubble stream and opposite to a continuous LED light source (Fig. 4). The recordings were performed at 70 kHz frame rate with an exposure time of 1 μs, using a camera lens of 200 mm focal length. The image sensor was cropped to 320x192 px² with a magnification factor of 0.78, resulting in a FoV of 8×5 mm². The volume flow rates of helium Q_{He} and air Q_{air} were varied for five combinations of BFS flow rates (Q_{BFS}), resulting in many visual observations and 530 recorded conditions for further analysis. Most of the results presented (310 recordings) are based on the NLR bubble generator, while the DLR designs are included only in the discussion of bubble size and production rate. Each recording consisted in ten cycles of 500 images realized with a time interval of 200 ms from each other. In this manner, ten uncorrelated cycles are analyzed with a sufficient number of images for an estimate of the bubble production rate.

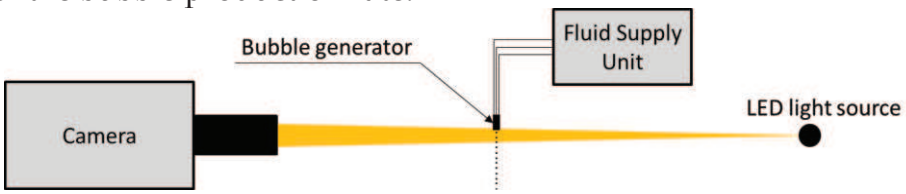

Fig. 4 Schematic illustration of the experimental set-up for bubbles shadow visualization.

4.1. Production regimes

For a given geometry and fluid properties, the combination of the fluids volume flow rates determines the type of bubble that is produced. A qualitative classification of the regimes of bubble production (Fig. 5) facilitates the discussion of the different phenomena involved in bubble formation. The main distinction made is to whether the bubble formation is in bubbling or jetting regime. Jetting is here defined as to the bubble formation (detachment location) occurring at least one bubble diameter downstream of the nozzle exit, otherwise, it is defined as bubbling. Other distinctions then follow to whether the production of bubbles is monodisperse,

i.e. periodic formation of bubbles with constant size, or visibly polydisperse. A specific regime is recognized when alternated production of two distinct population of monodisperse bubbles coexist (double-bubbling). Merging of bubbles can also be observed during double-bubbling or polydisperse production. Another different phenomenon is when a satellite bubble is formed in between the detachment point of bubble formation and the envelope of helium and soap. Although satellite bubbles are present in many situations, in most of the cases they are significantly smaller than the main bubbles and can be neglected. For ease of communication, double-bubbling, polydisperse-bubbling, large satellite bubbles and merging will be referred altogether as polydisperse-bubbling (unless differently specified). Monodisperse periodic bubble production will be referred simply as bubbling. Besides of polydisperse-bubbling, the population of bubbles is also polydisperse during jetting. Although monodisperse-jetting is a possible regime, such condition is often unstable and a slight change of flow rates may cause it to quickly transition into a polydisperse regime. Thus, from the perspective of a PIV user, the focus is on guaranteeing the bubbles are formed in the bubbling regime.

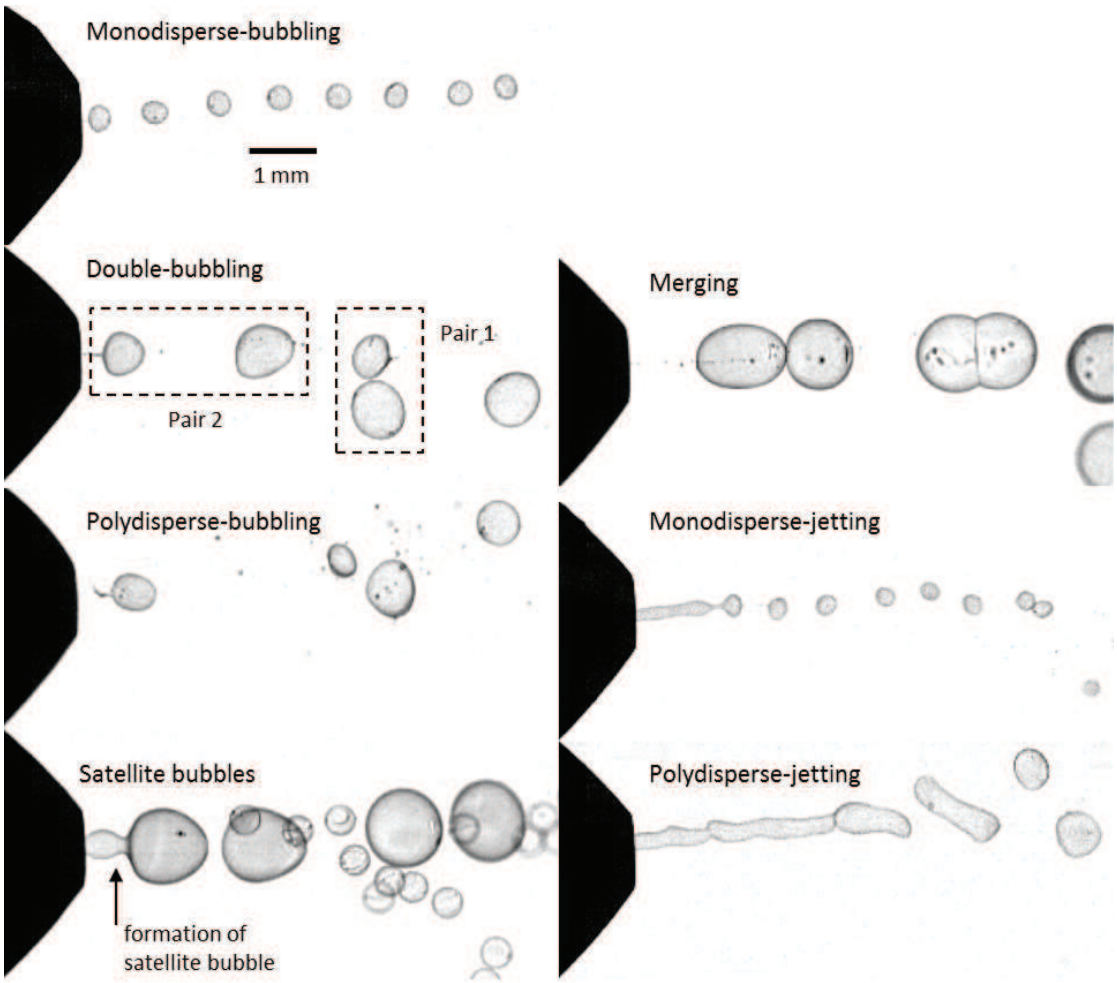

Fig. 5 Visualization of production regimes

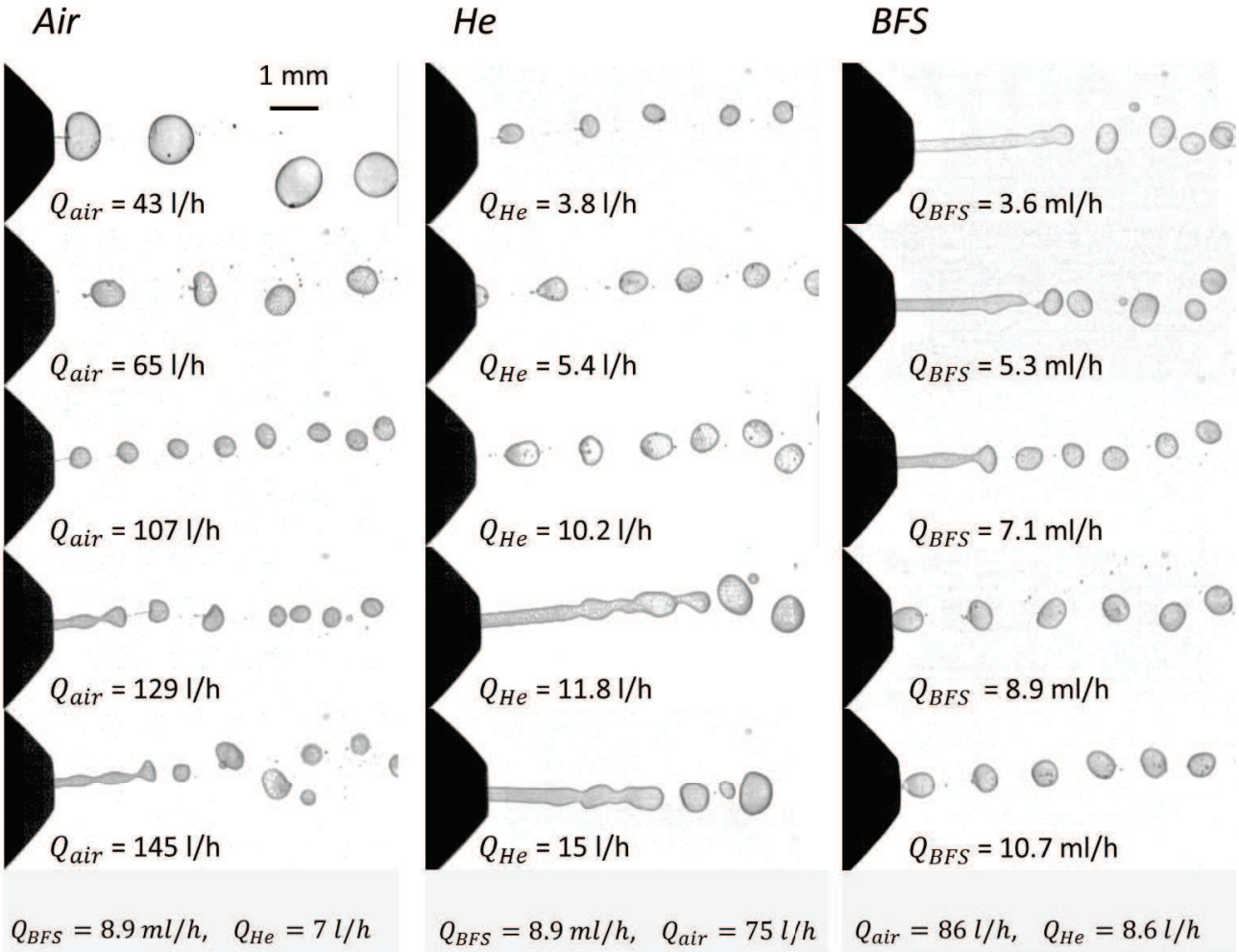

Fig. 6 Effect of flow rate variation in the bubble generation

Polydisperse-bubbling occurs mostly for low air flow rates and can be easily avoided through increasing the air flow rate (Fig. 7). Jetting may be avoided through observation of its occurrence in relation to the imposed flow rates. The effect of volume flow rate variation is observed for independent increase of air, helium and soap volume flow rate, while keeping the flow rates of the other two fluids constant (Fig. 6). Relatively low flow rates of air result in the generation of large bubbles in the bubbling regime. By increasing the air flow rate, the bubbles start to reduce in size and the distances between bubbles reduce, leading to an increase in the frequency of bubble production. At Q_{air} = 129 l/h, a jet extending about two bubble diameters away from the nozzle is formed, yet a rather monodisperse bubble size distribution is observed (monodisperse-jetting). As the volume flow rate of air is increased to Q_{air} = 145 l/h, the jet extends to about four bubble diameters downstream of the nozzle and the soap film breaks up into a polydisperse distribution of bubbles. Low flow rates of helium also result in the generation of bubbles in the bubbling regime, however, of rather small diameter. The increase of helium flow rate causes an increase in bubble size. However no clear change in the distance between

bubbles is observed. The transition to jetting (Q_{he} = 11.8 l/h) is more abrupt in this case and a long jet of about six bubble diameters is exhibited. The jet size is unsteady and the snapshot shown for Q_{he} = 15 l/h should not be interpreted as a reduction of jet length. For low flow rates of soap, on the other hand, the jetting regime is more likely to occur. Increasing the flow rate of BFS does not seem to affect either the bubble size or the frequency of bubble formation. The average jet length retracts as the flow rate of soap is increased and the bubble production regime becomes less disperse until it falls back into regular bubbling at Q_{BFS} = 8.9 ml/h.

4.2. Production regimes envelope

A systematic procedure is implemented, in which the volume flow rates of soap and helium are fixed while Q_{air} is increased from the first working condition till beyond the transition point from bubbling to jetting. The latter varies for different flow rates of helium and soap. The mapping of production regimes (shown in Fig. 7) is therefore given separately for experiments at a fixed value of Q_{BFS}.

For low Q_{BFS}, the region where the bubble generator is bubbling is very limited. For higher values of Q_{BFS} the range of air and helium flow rates yielding bubbling regime becomes significantly wider. The previous observation that jetting is present for high gas flow rates and low BFS flow rates becomes evident in these maps. Besides, the intersection of the neutral buoyancy condition (Q_{he} = 940 Q_{BFS}), represented as a black line, with the bubbling region show the desired working region. While meeting these two criteria, the choice of the flow rates becomes restricted. If the soap flow rate is increased further than 11 ml/h, a significant increase of soap spitting has been observed. Furthermore, it also caused more frequent occurrence of intermittent bubble production, i.e. the bubble generator works only a percentage of the time and the bubble production rate is reduced.

5. Bubble production rate and size

The bubble production rate is measured from the shadow visualization experiments. A detection and tracking algorithm renders the bubble velocities and counts the number of bubbles produced during each cycle. The bubbles are tracked from the nozzle exit until they leave the frame. The production rate in a single cycle is then calculated as

$$f_{cycle} = \frac{n}{(N-1)} f_c \qquad (4)$$

in which n is the number of generated bubbles in one cycle, N is the number of images per cycle and f_c is the camera acquisition frequency. The bubble production rate f is then defined as the average of f_{cycle} of all recorded cycles.

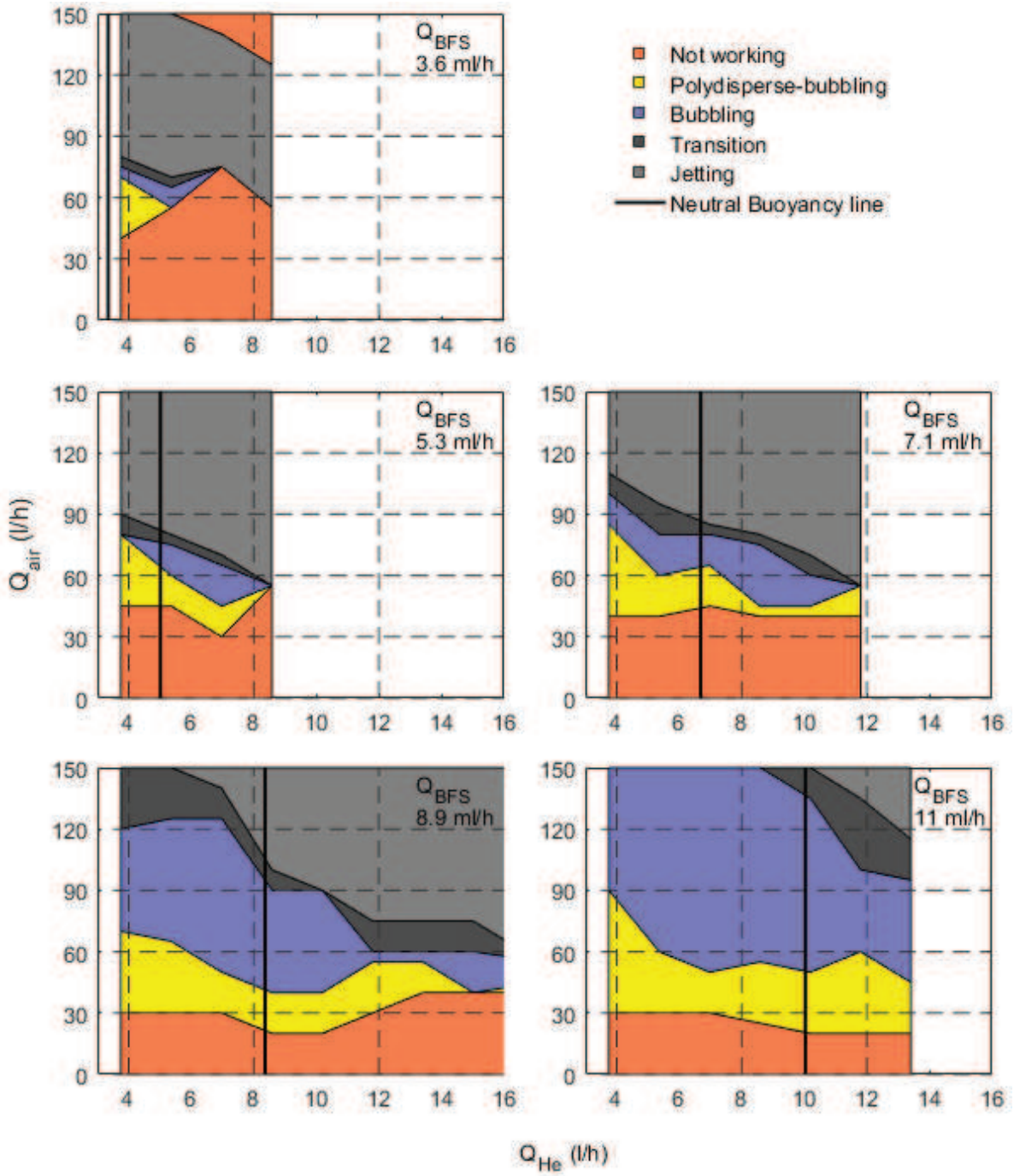

Fig. 7 Two-dimensional maps of bubbling and jetting regimes for varying flow rates.

The bubbles close to the nozzle are not yet of spherical but rather of oval shape, slightly elongated along the jet axis direction. The bubble size is thus calculated by fitting an ellipse to the bubble image edge and then assuming it to be an ellipsoid in three-dimensional space. The two smaller semi-axes are assumed to be equal for symmetry reasons. The bubble volume is then calculated as

$$V_p = 4\pi a b^2 \qquad (5)$$

in which a and b are the ellipse semi-major and semi-minor axes, respectively. The bubble diameter is then estimated for the reference condition of the bubble reaching spherical shape, which becomes valid further away from the nozzle exit

$$d_p = \left(\frac{6}{\pi} V_p\right)^{\frac{1}{3}} \qquad (6)$$

Neglecting the soap film thickness, the volume of the bubble can be also determined by integrating the volume flow rate of helium during the bubble formation time ($1/f$). Assuming, constant flow rate, the bubble volume reads as:

$$V_p = \frac{Q_{He}}{f} \qquad (7)$$

This relation is confirmed experimentally for the NLR (d_o = 1mm) (Fig. 8) and DLR (d_o = [0.75, 1.00, 1.50] mm) bubble generators. The good agreement of the data indicates that eq. (7) holds independently of bubble generator geometry.

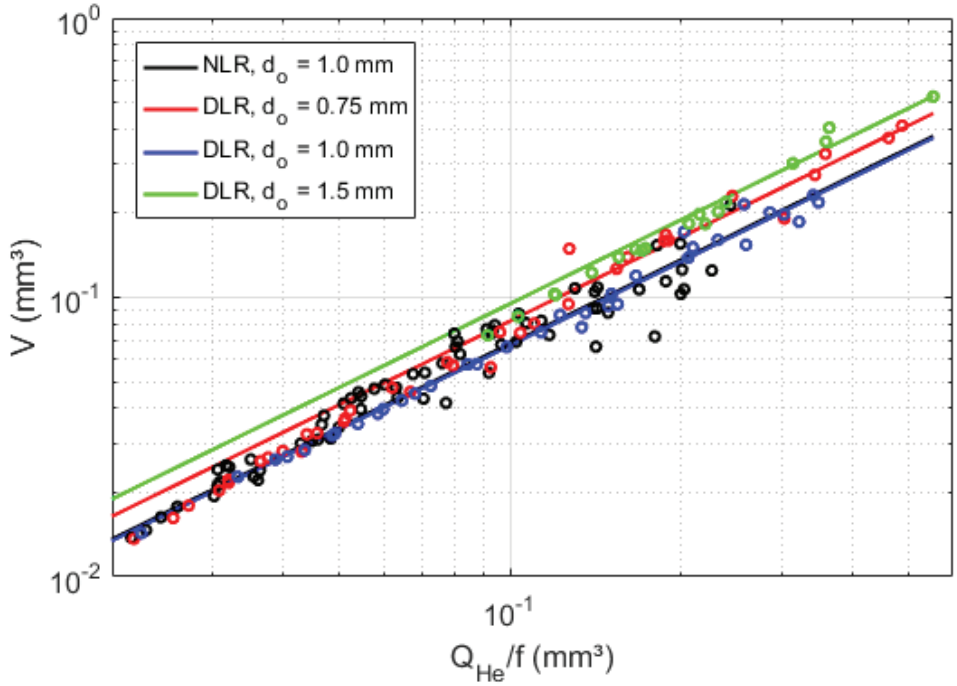

Fig. 8 Bubble volume vs. frequency

The formation time ($1/f$) is unknown, and it depends upon the parameters governing the film stability. From the flow visualizations it is observed that f is mainly affected by the air volume flow rate. The increase of Q_{air} reduces the bubble size and increases the bubble production rate. The latter is probably due to a reduction of the jet cross section area A_{jet}. A reduction of the radius of the envelope facilitates for surface tension forces to overcome the inertia forces and form a bubble in a shorter period of time.

The results show a linear dependence of production rate with volume flow rate of air (Fig. 9, left). Variations in the volume flow rates of helium and soap showed little influence in the bubble formation time. Although, part of the data dispersion seems to be explained by the different soap flow rates (not shown). Besides, it becomes evident that the bubble generator geometry influences the formation time. A complete analysis of the non-dimensional parameters governing this dependence has yet to be performed. Nevertheless, the data strongly indicates that when considering different orifice diameters for the same nozzle (DLR generator), the relation between f and Q_{air}/d_o collapses into a single curve.

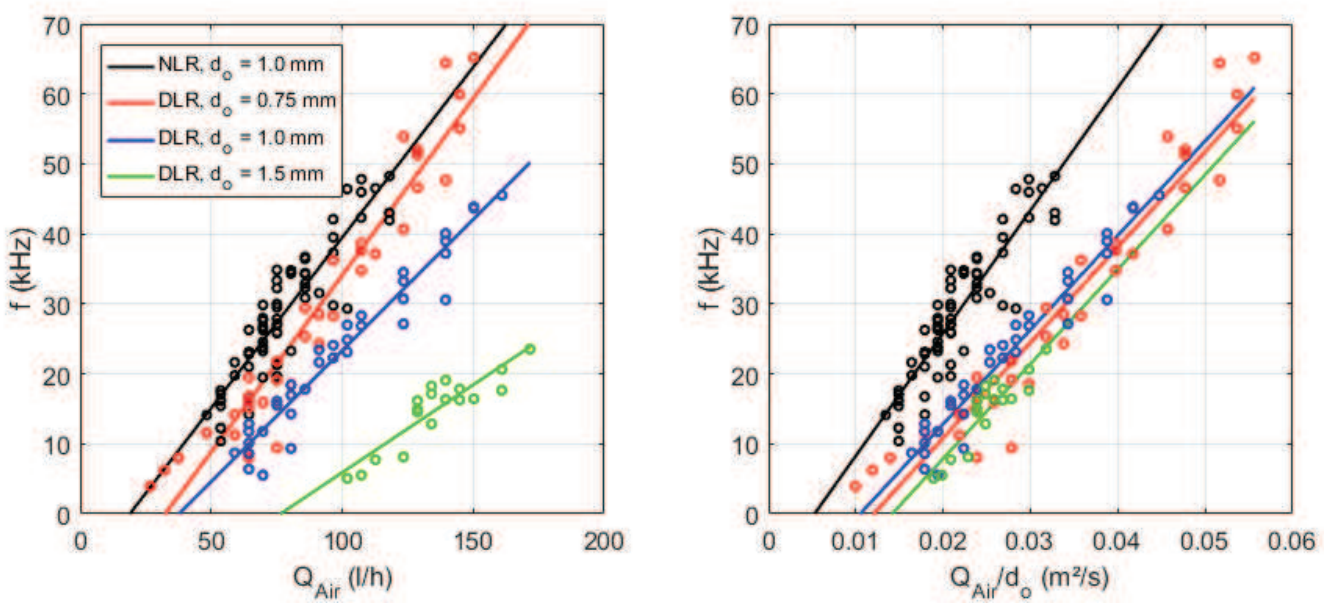

Fig. 9 Bubbles production rate as a function of air flow rate.

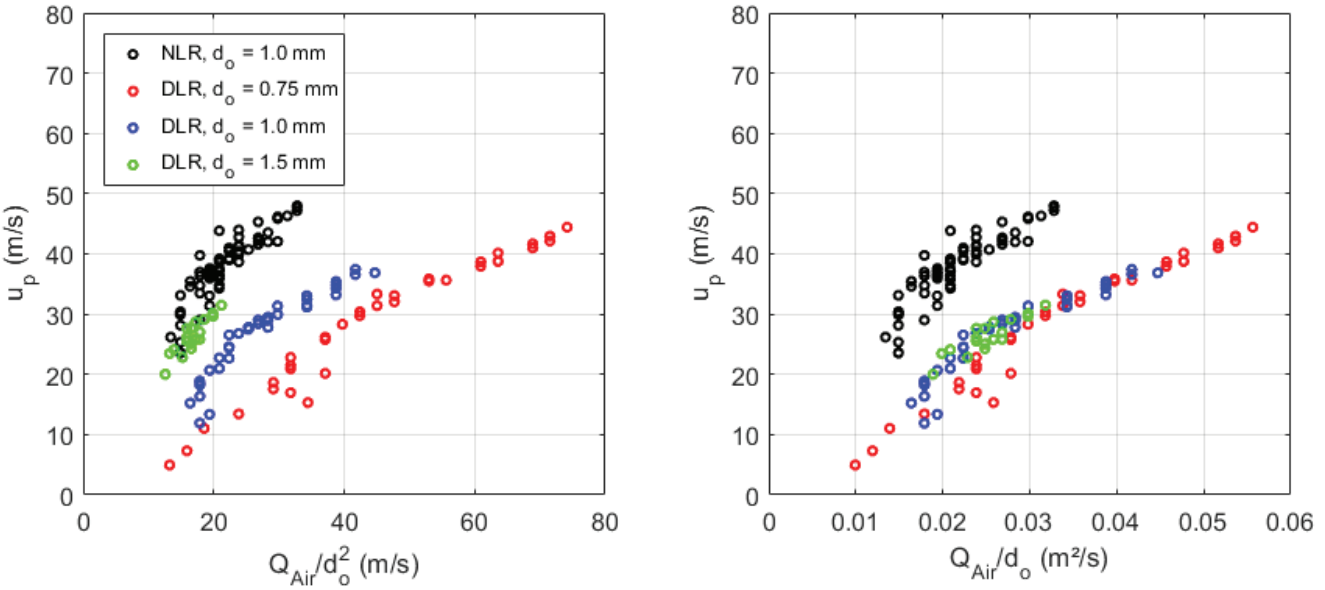

Fig. 10 Bubble velocity as a function of air flow rate

The bubble production rate is also defined as the ratio of bubble velocity and wave length of the bubble formation:

$$f = \frac{u_p}{\lambda} \qquad (8)$$

The bubble velocity is expected to vary mainly due to changes of air velocity u_{air}. At the orifice, the area of the annular cross section occupied by air was expected to scale with the orifice area $A_{air} \sim A_o$ and the air velocity therefore to scale as $u_{air} \sim Q_{air}/d_o^2$. Nevertheless, likewise the production rate, the measured bubble velocities for different orifice sizes show a better collapse with the ratio Q_{air}/d_o.

Combining eq. (7) with this empirical analysis it is concluded that the bubble volume is proportional to the ratio of helium and air flow rates and to the orifice diameter. The bubble diameter, consequently, scales as

$$d_p \sim \left(\frac{d_o Q_{He}}{Q_{air}}\right)^{\frac{1}{3}} \qquad (9)$$

The aforementioned proportionality is shown in Fig. 11. The data collapses well up to about $(d_o Q_{He}/Q_{air})^{\frac{1}{3}} = 0.5$. For larger values of the ratio the spread of the data increases especially for the DLR nozzles of 0.75 and 1.5 mm orifice diameters. For the larger diameter case, the bubble generator needs high Q_{air} to work properly since the orifice area has more than doubled in

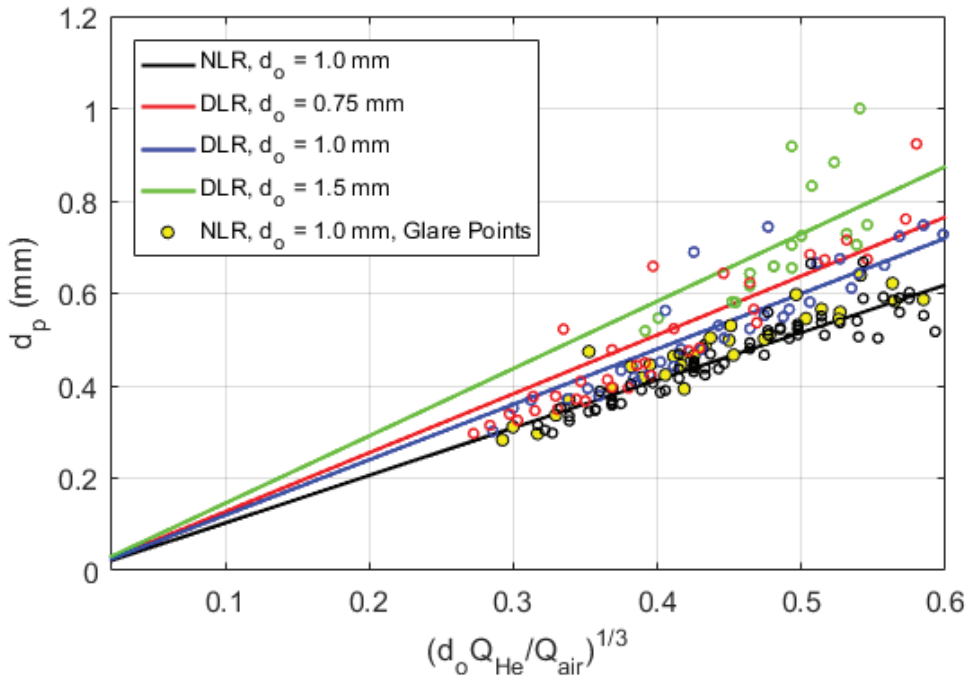

Fig. 11 Volumetric bubble size is linearly proportional to the ratio of inner and outer flow rates. Experiments correspond to the NLR bubble generator in the bubbling regime.

comparison to the reference d_o = 1 mm. Besides, larger bubbles are more prone to deformation and deviate from the spherical shape for a longer time while coming out from the orifice. The latter phenomenon might affect the accuracy to which the bubble size is determined. Both the data from the cylinder experiment (bubble diameter estimation from glare points) and from shadow visualization are plotted together. No significant difference is observed between the two methods.

From the current experiments it is deduced that $f = f(Q_{air}, d_o)$ and $d_p = d_p(Q_{air}, Q_{He}, d_o)$. From a PIV user perspective, it is useful to summarize these results by showing frequency and bubble diameter together as a function of air and helium volume flow rate isolines. The latter is shown for the NLR nozzle (d_o = 1 mm, Fig. 12). In this manner, one can easily select the gases flow rates from the desired frequency and diameter. The soap flow rate comes then from the empirical neutral-buoyancy relation (Q_{He}/Q_{BFS} = 940). And as a last check, Fig. 7 serves as a guide for verifying the present production regime for the chosen flow rates.

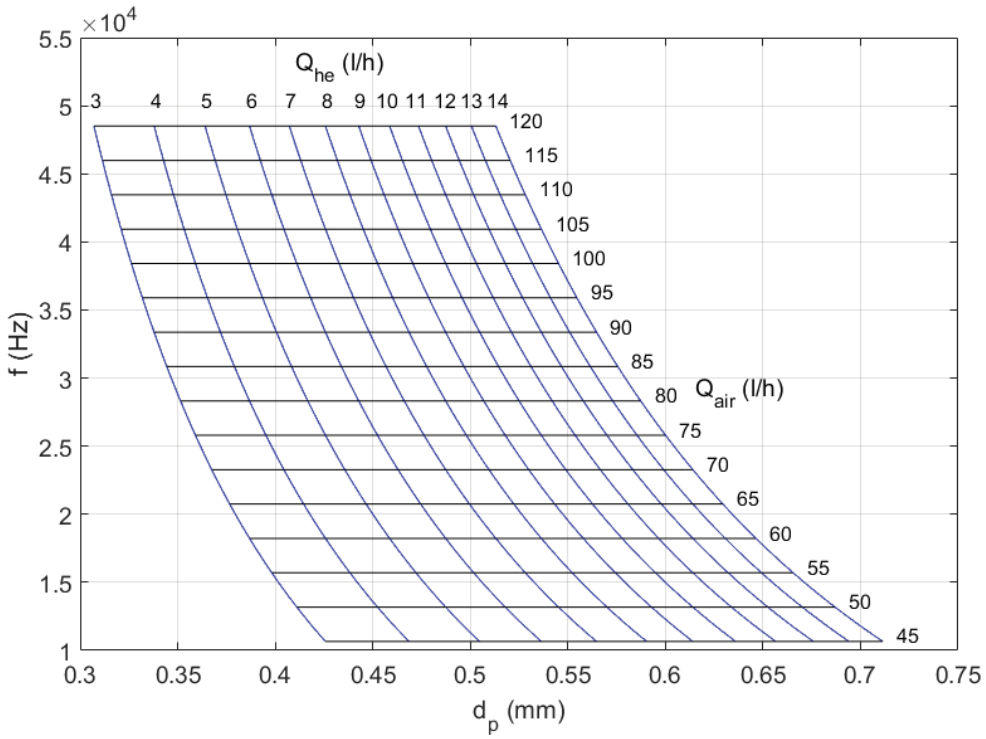

Fig. 12 HFSB production rate and diameter as a function of air and helium flow rates

6. Conclusions

The neutral buoyancy condition, which guarantees HFSB behave as PIV flow tracers, can be met by simply setting the helium and soap flow rates. It was found empirically that this condition is met when Q_{He}/Q_{bfs} = 940. This approaches to a theoretical prediction ($Q_{He}/Q_{bfs} \cong$ 1,080), with the difference being most likely due to soap spillage observed in the real process.

Several bubble production regimes are present and vary with the fluids flow rates. The production of HFSB in the bubbling regime results in lower variation of bubble size and a periodic bubble formation. Increasing the flow rate of gases or decreasing the flow rate of soap favors transition from bubbling to jetting, where a polydisperse distribution of bubbles is present. A broad mapping of such conditions as a function of flow rates has been presented.

The bubble production rate during bubbling regime was found to increase linearly with air volume flow rate. A linear relation between frequency and Q_{air}/d_o was found to be independent of orifice sizes. As a consequence of such relation, the bubble volume was found to be proportional to $d_o Q_{He}/Q_{air}$. A full non-dimensional analysis has yet to be performed. The empirical relations found in this study provide a PIV user with a useful guide on how to generate monodisperse neutrally-buoyant HFSB with pre-selected diameter and production rate.

References

- Bosbach J, Kühn M and Wagner C (2009) Large scale particle image velocimetry with helium filled soap bubbles. Exp Fluids 46: 539
- Caridi GCA, Ragni D, Sciacchitano A and Scarano F (2016) HFSB seeding for large scale tomographic PIV in wind tunnels. Exp Fluids 57: 190
- Caridi GCA (2018) Development and application of helium-filled soap bubbles for large-scale PIV experiments in aerodynamics, PhD Thesis. doi:10.4233/uuid:effc65f6-34df-4eac-8ad9-3fdb22a294dc
- Dehaeck S, van Beeck JPAJ., Riethmuller ML (2005) Extended glare point velocimetry and sizing for bubbly flows. Exp Fluids 39:407–419
- Faleiros DE, Tuinstra M, Sciacchitano A, Scarano F (2018) Helium-filled soap bubbles tracing fidelity in wall-bounded turbulence. Exp Fluids 59
- Kähler C, Sammler B, Kompenhans J (2002) Generation and control of tracer particles for optical flow investigations in air. Exp Fluids 33, 736–742.
- Kerho MF, Bragg MB (1994) Neutrally buoyant bubbles used as flow tracers in air. Exp Fluids 16:393
- Mei R (1996) Velocity fidelity of flow tracer particles. Exp Fluids 22: 1
- Morias KLL, Caridi GCA, Sciacchitano A and Scarano F (2016) Statistical Characterization of Helium-Filled Soap Bubbles Tracing Fidelity for PIV, 18th International Symposium on the Application of Laser and Imaging Techniques to Fluid Mechanics, Lisbon
- Okuno Y, Fukuda T, Miwate Y and Kobayashi T (1993) Development of three dimensional air flow measuring method using soap bubbles. JSAE Review 14(4) pp. 50-55

- Pounder E (1956) Parachute inflation process, Wind-Tunnel Study WADC Technical report 56–391, Equipment Laboratory of Wright-Patterson Air Force Base pp. 17–18, Ohio, USA
- Raffel M, Willert CE, Wereley ST, Kompenhans J (2007) Particle Image Velocimetry -A Practical Guide, 2nd ed, Springer, Berlin
- Scarano F, Ghaemi S, Caridi GCA, Bosbach J, Dierksheide U and Sciacchitano A (2015) On the use of helium filled soap bubbles for large scale tomographic PIV in wind tunnel experiments.